# RECIRCULATORY FLOW VISUALIZATION IN HELICOPTER FLIGHT MODES

Arthur William Nelson

United States
Naval Postgraduate School

# THESIS

## RECIRCULATORY FLOW VISUALIZATION IN HELICOPTER FLIGHT MODES

by

Arthur William Nelson, III

Thesis Advisor: J.A.J. Bennett

September 1971

Approved for public release; distribution unlimited.

# Recirculatory Flow Visualization in Helicopter Flight Modes

by

Arthur William Nelson, III
Lieutenant, United States Navy
B.S., United States Navy Academy, 1964

Submitted in partial fulfillment of the
requirements for the degree of

MASTER OF SCIENCE IN AERONAUTICAL ENGINEERING

from the

NAVAL POSTGRADUATE SCHOOL
September 1971

# ABSTRACT

The classical working states of the airscrew were studied employing the three-dimensional flow visualization tunnel at the Naval Postgraduate School, Monterey, California. The various states were simulated in an attempt to gain insight into some of the present problems in helicopter rotor design. This method was extended to include two particular phenomena, the critical part of the vortex ring state and Mangler's distribution of induced velocity about a rotor in the helicopter mode. Using a feasible distribution ascertained from the flow visualization, the induced velocity distribution was calculated for several points in the vortex ring state.

# TABLE OF CONTENTS

# TABLE OF SYMBOLS

Specified values are used in subsequent calculations.

| | |
|---|---|
| $V_o$ | steady velocity of ascent or descent |
| $v$ | induced velocity at blade element dr |
| $r$ | radical distance of element dr from rotor axis |
| $R$ | rotor radius = 30 feet |
| $B$ | number of blades |
| $C$ | chord of blade (considered constant) |
| $\theta$ | geometric blade angle measured from no-lift line = .07 radians |
| $\alpha$ | angle of attack measured from no-lift line |
| $\phi$ | $\alpha - \theta$ or $u/\omega r$ |
| $\omega$ | angular velocity of blades, considered constant = 21 radians/sec |
| $\sigma$ | solidity or ratio of blade area to disk area $BC/\pi R = .05$ |
| $\rho$ | density of air |
| $C_\ell$ | elemental coefficient of lift |
| $T$ | thrust along the shaft |
| $dT$ | elemental thrust due to B blade elements at radial distance r |
| $x$ | non-dimensional rotor radius $r/R$ |
| $A$ | slope of lift curve = 3 |
| $u$ | flow through rotor; $V_o - v$ for upwash; $v - V_o$ for downwash |

# I. INTRODUCTION

The last decade has witnessed the emergence of the helicopter's increasingly important role in military and civil aviation. Militarily, it has become the backbone of the Army's tactical doctrine. The other services have also found it increasingly reliable in their own particular operations. Civil aviation has barely scratched the surface of the potential applications of the helicopter. It has been used as a shuttle service between large urban areas and their major airports. Recent studies have shown that this service could be profitably extended to short and medium range operations, in competition with the passenger jets. Like the proverbial tortoise and the hare, the helicopter, which can transport the passenger from door-step to door-step, is often a faster mode of transportation than the jet liner.

The demand for faster and more versatile helicopters has renewed interest in low speed aerodynamics after a long emphasis on supersonic, hypersonic, and space applications.

The flow field of a helicopter rotor is extremely difficult to model mathematically. The periodicity of the rotor, areas of reverse flow, and the non-uniformity of the inflow are only a few of the problems which are confronted when trying to calculate flow and performance parameters.

One tool used to aid in these calculations is flow visualization. From a visual study of the flow in a rotor system, a feasible mathematical expression for the different variables may be determined. In this paper flow visualization is used to examine the working states of the rotor and to assist in the calculation of induced velocity in the vortex ring state, that is to say, recirculatory flow at negative speeds of advance.

# II. FLOW VISUALIZATION

With an increasing interest in STOL/VSTOL aircraft, some of the unsolved low speed aerodynamic problems, which have fallen by the wayside in the space age, are receiving more attention. As discussed previously, one of the more useful tools in selecting a mathematical model is flow visualization. With this in mind a flow visualization facility has recently been completed at the Naval Postgraduate School. This facility is modeled after the one described in Reference 5.

Several methods were attempted to obtain the cloud used as the visualization medium. The most effective was found to be the vaporization of silicone-based turbine solvent. This fluid produces a dense white coherent cloud. Low-pressure air forces the fluid to drop on a heated surface in a locally manufactured cloud generator heated by a 2400-watt hot plate. As the vaporized fluid collects in the top of the generator, it is forced by the low air pressure through a nozzle directed over the blade. The rotor is a one-bladed device driven by a variable speed electric motor. The speed of the blade and tunnel as well as control of the visualization devices is centrally located near the observation window. A strobe light with a variable flasher allowed the blade to be viewed once every revolution. Since the vortices are being shed at essentially the same

# [illegible]

[illegible]

[illegible]

[illegible]

frequency as the blade rotates, they also appear to remain stationary in the free stream. Pictures of the flow were taken with a Polaroid camera using ASA 10,000 film. Figure 2 shows a schematic of the tunnel. Figure 1 is a picture of the symmetrical cross-section blade mounted horizontally. The blade is counterbalanced to insure rotor vibrational stability.

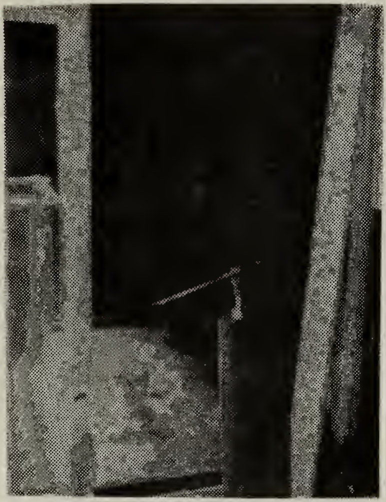

Figure 1. Rotor Used in Horizontal Segments of Visualization.

[illegible]

[illegible]

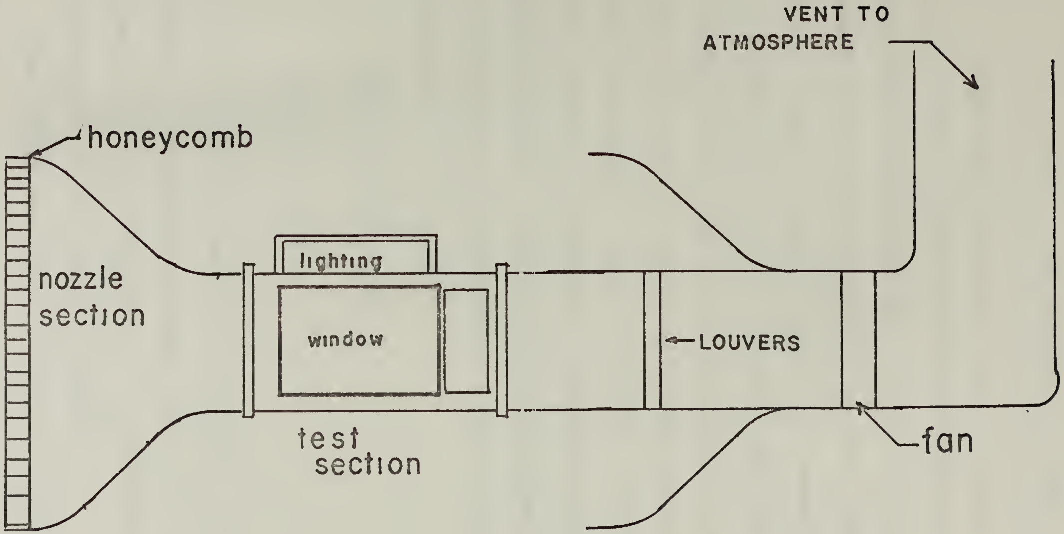

Figure 2. Schematic of the Naval Postgraduate School Flow Visualization Tunnel.

## III. THE GLAUERT EMPIRICAL CURVE

In 1925 C.N.H. Lock and others proposed to augment the "vortex theory of airscrews" with empirical data. Since this theory breaks down for a range of working conditions between zero speed of advance and some negative speed of advance, a two-bladed airscrew was tested at angles of attack below the stall. The data from this airscrew was used to fill the gap in the range where the theory did not apply. In 1926 H. Glauert extended Lock's analysis to cover the complete range of working conditions. The data which eventually evolved is commonly referred to as Glauert's empirical curve. This curve is expressed in terms of two non-dimensional coefficients, F and f, defined by the following relationships:

$$\frac{dT}{dr} = 4\pi\rho \ (V_o - v)^2 F \tag{1}$$

$$\frac{dT}{dr} = 4\pi\rho \ V_o{}^2 f \tag{2}$$

$V_o$ is the speed of ascent or descent, v is the induced velocity at the blade element, and r is the distance of the element from the rotor axis. The results of these two investigations are given in Figure 3.

The helicopter rotor in some instances acts as a propeller, notably in the hover and in vertical ascent or descent. The conventional anti-torque or tail rotor is

subjected to the same type of flow when the helicopter is in sideward flight. Therefore the empirical data is of interest in the study of helicopter aerodynamics. In the following pages the three working states of the rotor will be discussed and flow visualization pictures will be used to substantiate the discussion.

## A. THE NORMAL PROPELLER STATE

The normal propeller state is the region on Glauert's empirical curve (Fig. 1) which starts at a point where

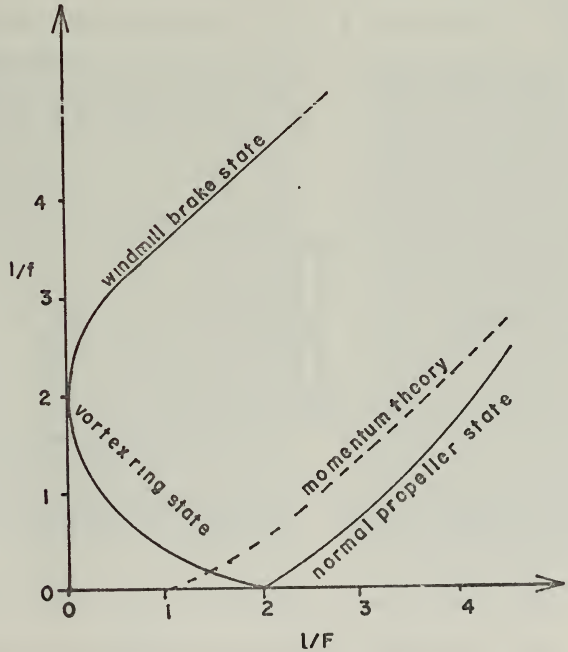

Figure 3. Glauert's Empirical Curve.

$1/f = 0$ and where $1/F$ has one of several values. According to Glauert's curve $1/F = 2.0$; by the momentum theory $1/F = 1.0$. In practice $1/F$ is between these two extremes, normally around the value of 4/3. The normal propeller state extends to the right as values of $1/F$ and $1/f$ increase. This state can be represented as shown in Figure 4, T being the thrust of the rotor and u the flow through the disk. Initially, in the hover mode, $V_o = 0$ and $u = v$. As power is increased, the helicopter ascends with a speed $V_o$. The flow through the rotor is now $V_o + v$ and, from the momentum theory, is $V_o + 2v$ downstream. As the speed of ascent increases, the value of $u/V_o \rightarrow 1$ since $u/V_o = \frac{V_o+v}{V_o} = 1+v/V_o$. In the limiting case of $u/V_o = 1$, $1/f = 1/F = \infty$. Therefore $f = F = T = 0$ and $u = V_o$.

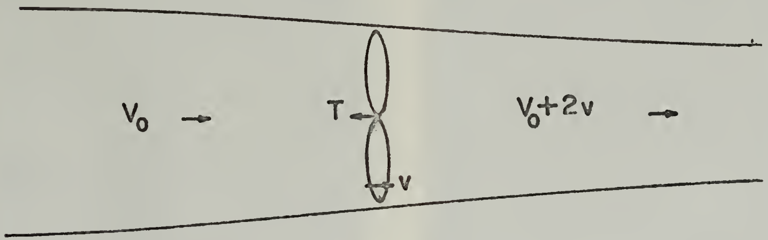

Figure 4. Diagram of Normal Propeller State.

The photographs in Figure 3 were taken with the rotor arranged to simulate the normal propeller state. The rotor axis is mounted parallel to the free stream which flows from

left to right. The blade is rotating clockwise when viewed along the free stream vector. The thrust and induced velocity vectors are in the same direction as depicted in Figure 4. The tip vortices are obvious as is the vena contracta. The decrease in slipstream area downstream indicates an increase in velocity. In Figure 5-b the start of cyclonic tails which originate in the eye of the vortex are plain. Although not obvious in the second picture, these tails or trailing vortex lines extend downstream of the rotor in a sprial pattern, the visible series of tip vortices being simply the result of vortex flow around each spiral vortex line.

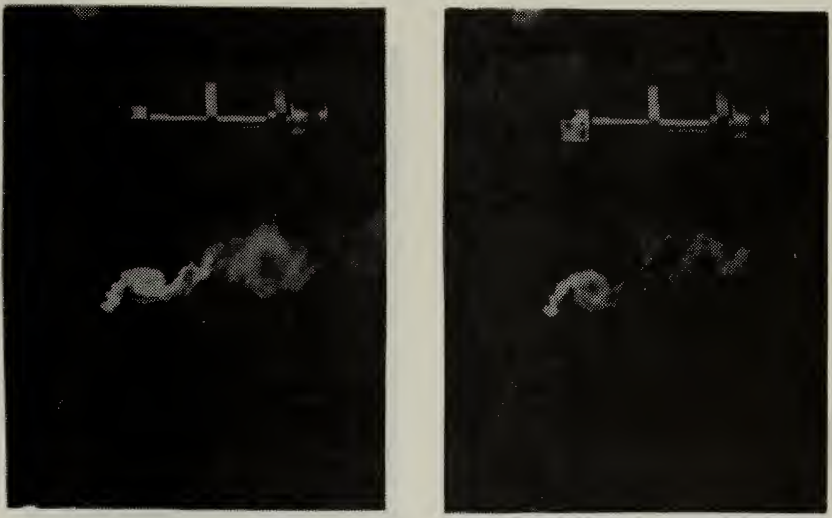

a.

b.

Figure 5. Normal Propeller State.

### 1. The Hover

As discussed previously, one of the limiting cases of the normal propeller state is the point where 1/f = 0 and 1/F = 2. This is the hover mode and presents a severe challenge to the aerodynamicist in his attempt to predict rotor performance. The induced velocity is extremely important in this region because in a hover the induced power is approximately two thirds of the hover power for a helicopter with a conventional figure of merit. Previous attempts to calculate the rotor performance have not been very accurate because the vorticity from a blade is not swept away from the disk and strongly influences flow on the preceding blade. As the number of blades increases,

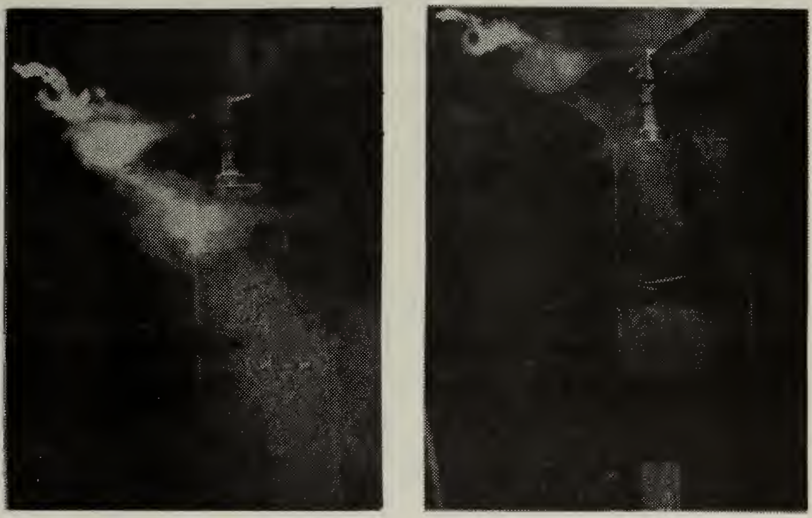

a. b.

Figure 6. The Hover.

this effect becomes more pronounced. Figure 6 shows the blade mounted horizontally, with $V_o = 0$ to simulate the hover mode. In the pictures the trail of vorticity is quite evident and is still in close proximity to the plane of the disk, even though the blade is past the beam position. With a four-bladed rotor, the next blade would be strongly affected by this vorticity. The pictures also show the vortices extending to the periphery of the disk and indicates the vena contracta under the rotor.

## B. THE VORTEX RING STATE

If the helicopter is in a hover and power is decreased, it begins to descend under power. This is the vortex ring state and is represented empirically on Glauert's curve as the branch extending from the hover point, which has previously been discussed, to the so-called point of ideal autorotation, that is, $1/f = 2.0$ and $1/F = 0$. Schematically it is represented by the following diagram:

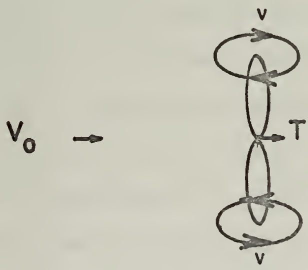

Figure 7. Diagram of Vortex Ring State.

In this case the thrust vector is in the same direction as the relative velocity in a descent. Initially, as power is reduced, the induced velocity v is much larger than the sinking speed and $u/V_o$ is negative and large. As the sinking speed increases, $u/V_o$ becomes smaller and the induced velocity does not travel as far upstream before it is dissipated by the free stream. With further increase in $V_o$, the tip vortex flow is driven downstream (with respect to $V_o$) and is then drawn into the rotor flow. This recirculatory phenomenon starts at the rotor tips and moves inboard. At some sinking speed, $V_o$, the induced velocity can not escape from the plane of the rotor disk and the whole disk becomes embraced in turbulent flow.

In Figure 8 the angle of attack has been modified to allow the test section to simulate a rotor in the vortex ring state. The free stream moves from left to right and, this time, the thrust vector points in the same direction. Figure 8-a simulates the rotor at a very low sinking speed. The tip vortices are clearly seen. The cloudy background indicates that the induced velocity has been dissipated and the flow is downstream outboard of the rotor disk. Figure 8-b shows the critical part of the vortex ring state. The blade is enveloped in a turbulent flow, the pattern of which is fluctuating periodically. The phenomenon results in a loss of thrust and severe vibration of the rotor.

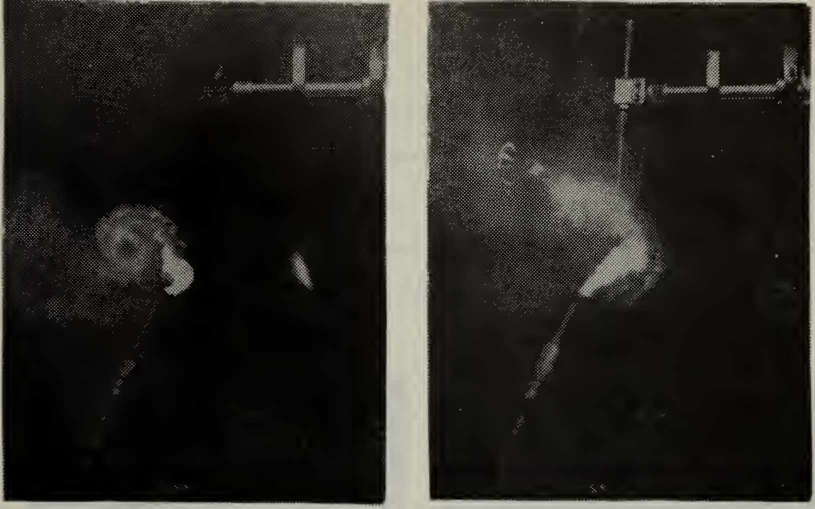

a. b.

Figure 8. Vortex Ring State.

## C. THE WINDMILL BRAKE STATE

The last of the working states is the windmill brake state and occurs when the blades are extracting energy from the air. It is the upper branch of Glauert's curve from the ideal autorotation point to $1/f = 1/F = \infty$. Now $u = V_o - v$ and $u/V_o = 1 - \frac{v}{V_o}$. As $V_o$ increases, $u/V_o \to 1$. Schematically this state is shown below.

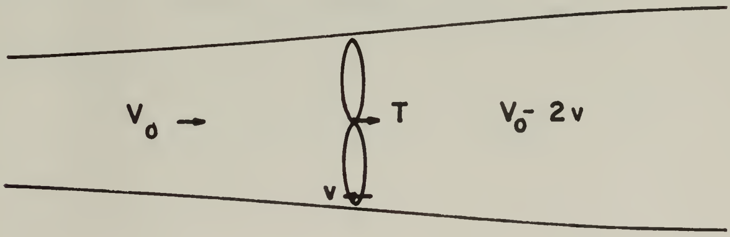

Figure 9. Diagram of Windmill Brake State.

Figure 10 is an extention of the previous pair of photographs except that the tunnel speed is increased above the value which caused the blade to be in the critical part of the vortex ring state. Both pictures clearly show that tip vortices are again formed and that the area downstream is greater than that upstream or the converse of the stream tube embracing the disk in the normal propeller state.

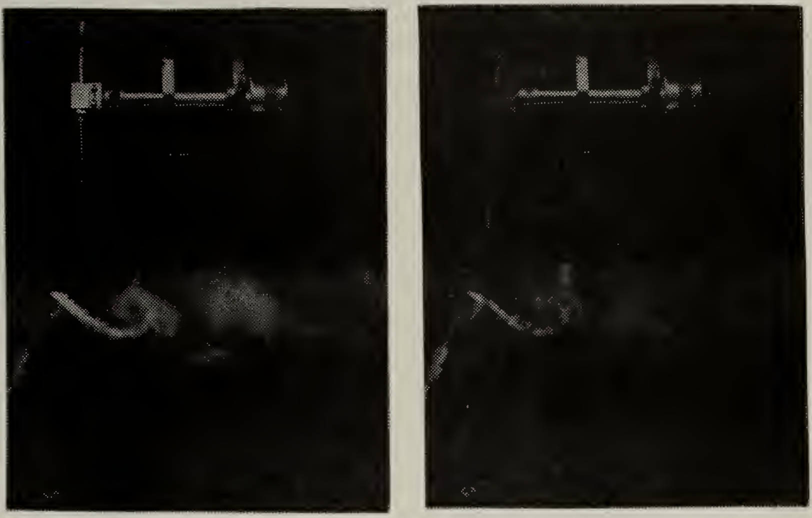

a.   b.

Figure 10. Windmill Brake State.

## IV. MANGLER'S DISTRIBUTION

Glauert's assumption that the induced velocity is distributed uniformly across the disk is fairly restrictive. In 1948 Mangler calculated an induced velocity distribution which was more general. He assumed that there was an infinite number of blades, allowing the rotor system to be replaced by a circular disk. He also assumed that the tip speed ratio was large. This rules out investigation of the region around the hover mode, which has already been pointed out as a critical area. Mangler selected a plausible loading over the disk (Fig. 11) and calculated the corresponding distribution of u.

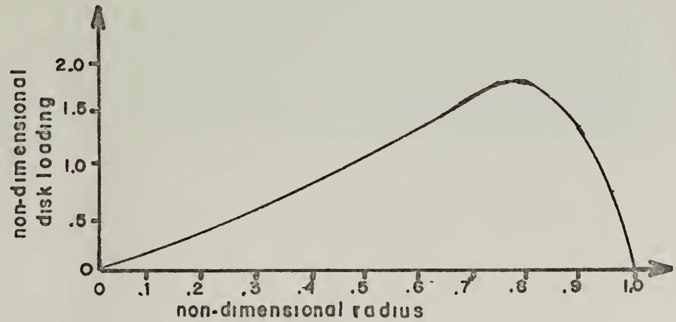

Figure 11. Non-dimensional Disk Loading.

The results are shown in Reference 4 for different values of disk incidence. The most significant deviation from Glauert's original assumption is that, since the disk is producing lift, there is circulation around the disk. Thus there is an upwash in the front of the disk. This phenomenon is shown clearly in Figure 12, there being an upwash in the front of the disk followed by a downwash. Notice also the vortices in the downwash through which the blades are passing.

a.

b.

Figure 12. Mangler's Distribution.

[illegible]

# V. CALCULATION OF THE LINEAR STEADY STATE VELOCITY IN THE VORTEX RING STATE

With the aid of smoke flow visualization, it is now possible to chose a plausible mathematical model in an attempt to calculate the induced velocity in the vortex ring state. These velocities will be determined by considering the data from Glauert's empirical curve and applying a method of analysis similar to that used by Bennett in Reference 1.

Consider Glauert's definition for the thrust coefficients:

$$\frac{dT}{dr} = 4\pi r\rho u^2 F \tag{1}$$

$$\frac{dT}{dr} = 4\pi r\rho V_o^2 f \tag{2}$$

u is the resultant flow through the elemental annulus and is expressed as $V_o - v$ in an area of upwash and $v - V_o$ in an area of downwash, both expressions being positive. To calculate the induced velocity, a new thrust coefficient $\overline{F}$ will be defined:

$$\frac{dT}{dr} = 4\pi r\rho v^2 \overline{F} \tag{3}$$

Dividing equation (1) by equation (2) yields

$$F = \frac{V_o^2}{u^2} f$$

Dividing equation (1) by equation (4) gives,

$$\bar{F} = \frac{u^2}{v^2} F \qquad (5)$$

Substituting equation (4) into equation (5),

$$\frac{\bar{F}}{f} = \frac{V_o^{\,2}}{v^2} \qquad (6)$$

Re-writing equation (4) and expanding u, noting that $(V_o - v)^2 = (v - V_o)^2$

$$\frac{f}{F} = (1 - 2v/V_o + v^2/V_o^{\,2} \qquad (7)$$

or

$$\frac{f}{F} = 1 - 2\sqrt{f/\bar{F}} + f/\bar{F} \qquad (8)$$

Solving for 1/F

$$\frac{1}{\bar{F}} = (\sqrt{1/f} + \sqrt{1/F})^2 \qquad (9)$$

For the range of values for 1/f and 1/F in the vortex ring state, the value of 1/F can be determined.

| $1/f$ | $1/F$ | $1/\bar{F}$ |
|---|---|---|
| 0.0 | 2.0 | 2.0 |
| .5 | 1.0 | 2.91 |
| .6 | .75 | 2.69 |
| .8 | .50 | 2.56 |
| 1.08 | .25 | 2.37 |
| 2.0 | 0.0 | 2.0 |

Now Glauert's curve becomes three dimensional. The projections are shown in Figure 13. The relationship between $1/\overline{F}$ and $1/f$ is approximated by a fourth degree least squares polynomial fit.

$$\frac{1}{\overline{F}} = a\left(\frac{1}{f}\right)^4 + b\left(\frac{1}{f}\right)^3 + c\left(\frac{1}{f}\right)^2 + d\left(\frac{1}{f}\right) + e \qquad (10)$$

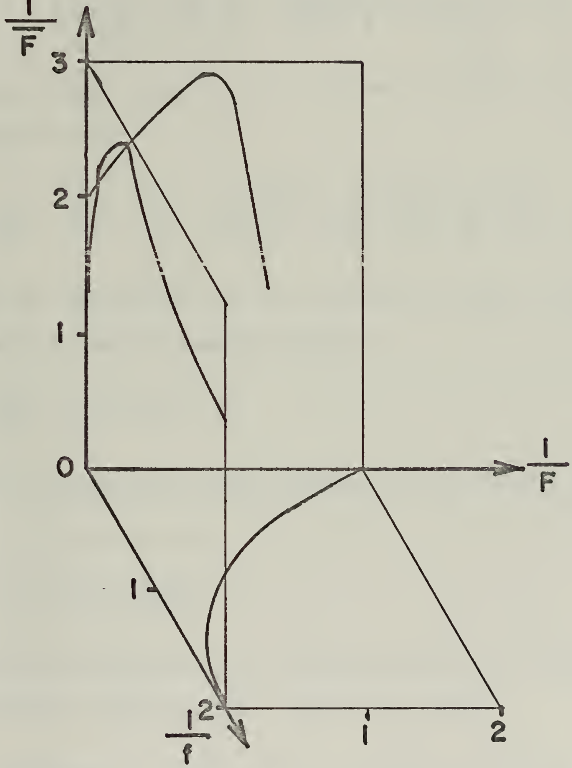

Figure 13. "Three Dimensional Glauert's Curve."

where $a = -2.96$

$b = 12.96$

$c = -18.76$

$d = 9.68$

$e = 1.38$

Solving for f, recalling that $\frac{1}{f} = \frac{v^2}{V_o^2 F}$

$$f = \frac{1}{e}\left[\frac{v^2}{V_o^2} + \frac{a}{\bar{F}^3}\frac{V_o^6}{v^6} - \frac{b}{\bar{F}^2}\frac{V_o^4}{v^4} + \frac{c}{\bar{F}}\frac{V_o^2}{v^2} - d\right] \tag{11}$$

Substituting into equation (2) and multiplying the terms in the brackets by $V_o^2$.

$$\frac{dT}{dr} = \frac{4\pi\rho r}{e}\left[v^2 + \frac{a}{\bar{F}^3}\frac{V_o^8}{v^6} - \frac{b}{\bar{F}^2}\frac{V_o^6}{v^4} + \frac{c}{\bar{F}}\frac{V_o^4}{v^2} - dV_o^2\right] \tag{12}$$

Consider an expression for the thrust in terms of airfoil and dynamic pressure considerations,

$$\frac{dT}{dr} = C_\ell BC\rho(\omega r)^2 \frac{1}{2} \tag{13}$$

Consider an elemental blade section, as in Figure 14.

$$C_\ell = A\alpha = A(\theta+\phi) \tag{14}$$

$$C_\ell = A(\theta + \frac{V_o - v}{\omega r}) \tag{15}$$

Substituting equation (15) into equation (13) and equating the result to equation (12), recalling that

$$\frac{R\sigma\omega^2 rAe}{4}\left(\theta + \frac{V_o - v}{\omega r}\right) = \left[v^2 + \frac{a}{F^3}\frac{V_o^8}{v^6} - \frac{b}{F^2}\frac{V_o^6}{v^4} + \frac{c}{F}\frac{V_o^4}{v^2} - dV_o^2\right] \tag{16}$$

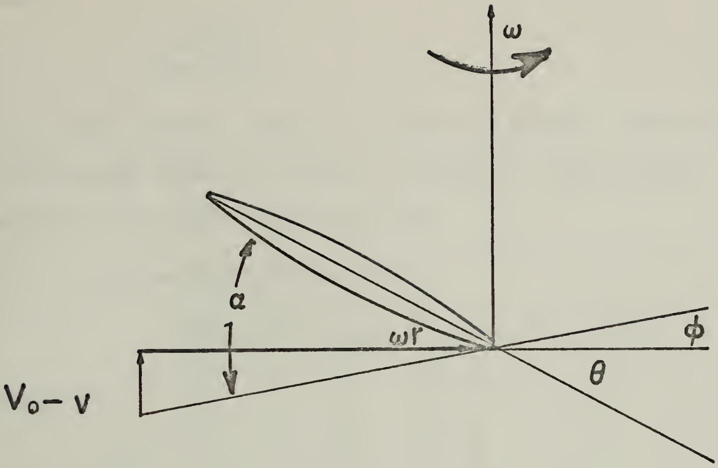

Figure 14. Elemental Blade Section.

Let $C_1 = \frac{R\sigma\omega Ae}{4}$

$$C_1\omega r\left(\theta + \frac{V_o - v}{\omega r}\right) = \left[v^2 + \frac{a}{\bar{F}^3}\,\frac{V_o^{\,8}}{v^6} - \frac{b}{\bar{F}^2}\,\frac{V_o^{\,6}}{v^4} + \frac{c}{\bar{F}}\,\frac{V_o^{\,4}}{v^2} - dV_o^{\,2}\right] \tag{18}$$

$$C_1\omega RX\theta + C_1V_o - C_1v = \left[v^2 + \frac{a}{\bar{F}^3}\,\frac{V_o^{\,8}}{v^6} - \frac{b}{\bar{F}^2}\,\frac{V_o^{\,6}}{v^4} + \frac{c}{\bar{F}}\,\frac{V_o^{\,4}}{v^2} - dV_o^{\,2}\right] \tag{19}$$

From equation (4)

$$u^2F = V_o^{\,2}f \tag{20}$$

$$(V_o^{\,2} - aV_ov + v^2)F = V_o^{\,2}f \tag{21}$$

$$F - 2\,\frac{v}{V_o}\,F + \frac{fF}{\bar{F}} = f \tag{22}$$

$$V_o = v\Delta \tag{23}$$

where

$$\Delta = \frac{2\bar{F}F}{\bar{F}F + fF - f\bar{F}}$$

$V_o$ is the constant speed of ascent or descent, and v is the average value of induced velocity. Substituting equation (23) into equation (18)

$$C_1\bar{F}^3\omega R\theta X + C_1\bar{F}^3 v\Delta - C_1\bar{F}v =$$

$$v^2\bar{F}^3 - a\Delta^8 v^2 - b\bar{F}v^2\Delta^6 - C\bar{F}^2 v^2\Delta^4 - d\bar{F}^3 v^2\Delta^2 \qquad (24)$$

Finally

$$K_1 v^2 + K_2 v + K_3 = 0 \qquad (25)$$

where

$$K_1 = (\bar{F}^3 + 2.96\Delta^8 - 12.96\bar{F}\Delta^6 + 18.76\bar{F}^2\Delta^4 - 9.68\bar{F}^3\Delta^2)$$

$$K_2 = C_1\bar{F}^3(1-\Delta)$$

$$K_3 = -C_1\bar{F}^3\omega\theta X$$

Knowing the blade characteristics, the location on the three-dimensional thrust curve, and the non-dimensional distance along the blade, the induced velocity may be calculated. Some typical values are given below in tabular form and graphically in Figure 15.

| 1/f | 1/F | $1/\bar{F}$ | $\Delta$ | $v_{average}$ | $V_o$ | comments |
|---|---|---|---|---|---|---|
| 0 | 2.0 | 2.0 | 0 | 24.5 | 0 | hover |
| .5 | 1.0 | 2.91 | .42 | 36.3 | 15.1 | condition one Fig.15 |
| .6 | .75 | 2.69 | .47 | 36.3 | 17.2 | |
| .8 | .50 | 2.56 | .56 | 33.1 | 18.5 | |
| 1.08 | .25 | 2.37 | .68 | 30.8 | 20.8 | condition two Fig.15 |
| 2.0 | 0 | 2.0 | 1.0 | 29.7 | 29.7 | "ideal autorotation" |

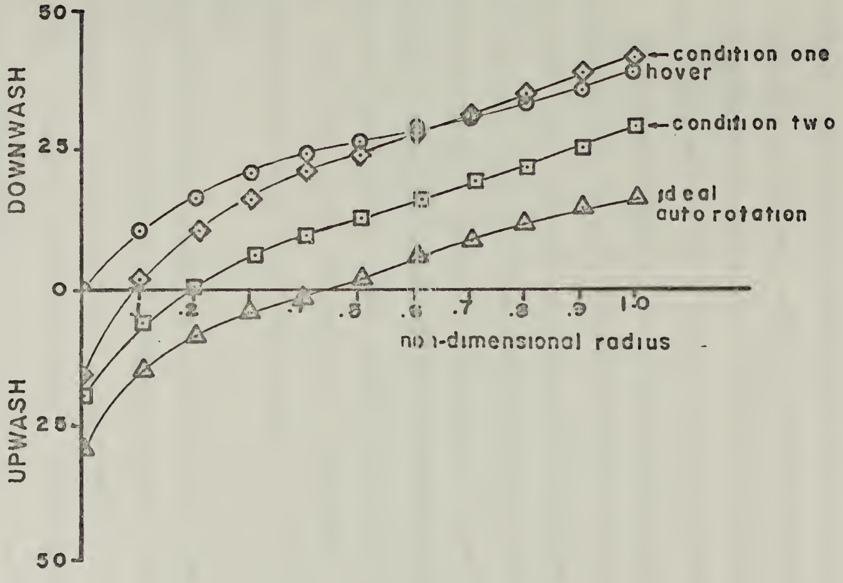

Figure 15. Flow Through Rotor for Various Points in the Vortex Ring State.

# VI. CONCLUSIONS

Flow visualization is an extremely useful tool which should be further exploited now that the facilities are available. More sophisticated methods of photography could be employed to record the vortices. Velocity measurements could be made in the wake with a device such as a hot-wire anemometer. These measurements, coupled with the photographs, could help clarify some questions about the complex flow in the rotor wake, as well as other flow problems.

Tip vortices exist in all the working states of the rotor just as an airplane wing has trailing vortices in all regimes of flight. In the hover mode the vortices can not escape from the plane of the rotor before the next blade comes along. The flow over the blade is, therefore, extremely complicated and rotor performance is difficult to calculate.

At some point in the vortex ring state, the steady state velocity of descent prevents the induced vortices from leaving the blade. The whole rotor is enveloped in vortex rings which are symmetric about the axis. This condition is unstable and these vortices are shed in a non-uniform manner.

Mangler's distribution is shown to be at least qualitatively correct. There is an upwash in front of the disk and the blade cuts through its own vorticity closer to

the hub. This blade-vortex interaction could cause undesirable vibrational effects.

The induced velocity distribution for several points in the vortex ring state was calculated. One of these points, "ideal autorotation," is not an empirical point, as is the others, but a theoretical point from Reference 3. The values obtained appear to be optimistic, that is, half the blade in upwash and half in downwash. As reported in Reference 1 the value where $V_o = v$ is much closer to the tip. This calculation takes into consideration the profile drag of the blade. As disk loadings become higher, the figure of merit approaches one, the profile drag will become less important and the distribution will approach the ideal case reported in this paper.

# BIBLIOGRAPHY

1. Bennett, J.A.J., "Rotary Wing Aircraft, Part II: Vertical Descent Without Power," *Aircraft Engineering*, p. 40-44, February 1940.

2. Advisory Committee for Aeronautics Reports and Memoranda No. 1026, *The Analysis of Experimental Results in the Windmill Brake and Vortex Ring States of an Airscrew*, by M.A. Glauert, February 1926.

3. Advisory Committee for Aeronautics Reports and Memoranda No. 1014, *An Extension of the Vortex Theory of Airscrews with Applications to Airscrews of Small Pitch, Including Experimental Results*, by C.N.H. Lock, H. Bateman, and H.C.H. Townsend, September 1926.

4. Advisory Committee for Aeronautics Reports and Memoranda No. 2642, *The Induced Velocity Field of a Rotor*, by K.W. Mangler and H.B. Squire, May 1950.

5. Naval Air Engineering Laboratory Report NAEL-ENG-6818, *The Three Dimensional Smoke Tunnel of the Naval Air Engineering Laboroatory in Philadelphia, Pennsylvania*, by Friedrich O. Ringleb, 10 July 1961.

# INITIAL DISTRIBUTION LIST

| | | No. Copies |
|---|---|---|
| 1. | Defense Documentation Center<br>Cameron Station<br>Alexandria, Virginia 22314 | 2 |
| 2. | Library, Code 0212<br>Naval Postgraduate School<br>Monterey, California 93940 | 2 |
| 3. | Professor J.A.J. Bennett, Code Zn<br>Department of Aeronautics<br>Naval Postgraduate School<br>Monterey, California 93940 | 1 |
| 4. | Chairman, Department of Aeronautics<br>Naval Postgraduate School<br>Monterey, California 93940 | 1 |
| 5. | LT Arthur William Nelson, III<br>391-A Ricketts Road<br>Monterey, California 93940 | 1 |

## DOCUMENT CONTROL DATA - R & D

*(Security classification of title, body of abstract and indexing annotation must be entered when the overall report is classified)*

| | |
|---|---|
| 1 ORIGINATING ACTIVITY *(Corporate author)*<br>Naval Postgraduate School<br>Monterey, California 93940 | 2a. REPORT SECURITY CLASSIFICATION<br>Unclassified |
| | 2b. GROUP |

3 REPORT TITLE

RECIRCULATORY FLOW VISUALIZATION IN HELICOPTER FLIGHT MODES

4 DESCRIPTIVE NOTES *(Type of report and, inclusive dates)*

Master's Thesis; September 1971

5 AUTHOR(S) *(First name, middle initial, last name)*

Arthur William Nelson, III; Lieutenant, United States Navy

| | | |
|---|---|---|
| 6. REPORT DATE<br>September 1971 | 7a. TOTAL NO. OF PAGES<br>34 | 7b. NO. OF REFS<br>5 |
| 8a. CONTRACT OR GRANT NO.<br>b. PROJECT NO.<br>c.<br>d. | 9a. ORIGINATOR'S REPORT NUMBER(S)<br>9b. OTHER REPORT NO(S) *(Any other numbers that may be assigned this report)* | |

10. DISTRIBUTION STATEMENT

Approved for public release; distribution unlimited.

| | |
|---|---|
| 11. SUPPLEMENTARY NOTES | 12. SPONSORING MILITARY ACTIVITY<br>Naval Postgraduate School<br>Monterey, California 93940 |

13. ABSTRACT

The classical working states of the airscrew were studied employing the three-dimensional flow visualization tunnel at the Naval Postgraduate School, Monterey, California. The various states were simulated in an attempt to gain insight into some of the present problems in helicopter rotor design. This method was extended to include two particular phenomena, the critical part of the vortex ring state and Mangler's distribution of induced velocity about a rotor in the helicopter mode. Using a feasible distribution ascertained from the flow visualization, the induced velocity distribution was calculated for several points in the vortex ring state.

| KEY WORDS | LINK A | | LINK B | | LINK C | |
|---|---|---|---|---|---|---|
| | ROLE | WT | ROLE | WT | ROLE | WT |
| ROTOR FLOW | | | | | | |
| VORTEX RINGS | | | | | | |
| GLAUERT CURVE | | | | | | |